Fast FBG Interrogator on Chip Based on Silicon on Insulator Ring Resonator Add/Drop Filters

Lorenzo Tozzetti, Francesca Bontempi, Anna Giacobbe, Fabrizio Di Pasquale, and Stefano Faralli, *Member, IEEE*

***Abstract*—A fast FBG sensor interrogator on chip based on SOI ring resonator (RR) filters is presented. The measurement of the Bragg wavelength shift is based on the detection of multiple signals at the output ports of the RR filter, providing fast dynamic strain measurement capabilities, fundamentally limited by the photodetector bandwidth and signal processing. The ring resonator resonance wavelength is tuned and fixed by an integrated heater and the ring acts as a passband filter for the reflected FBG spectrum. After a theoretical analysis of the interrogation method, which allows the optimization of the RR characteristics depending on the specific application and requirements, we present experimental results on a single RR based interrogation scheme applying high frequency dynamic strain up to 40 kHz. We also theoretically evaluate the performance of multi-ring resonators. The proposed scheme provides low cost, high scalability to mass-volume market applications as well as an extremely fast interrogation method.**

***Index Terms*—Fiber bragg grating, integrated photonics, optical fiber sensor, photonic integrated circuits, silicon on insulator.**

I. Introduction

FIBER Bragg Grating (FBG) sensors are attracting great attention in different industrial sectors such as structural health monitoring, energy production, conversion and storage, oil & gas, transportation, automotive, security, medical and biotech [1]–[6]. FBG sensors offer advantages compared to electronic sensors because they are compact, low weight, resistant to harsh environments, electrically passive, immune from electromagnetic interference, and a high number of FBG sensors can be multiplexed in a single optical fiber.

However, a full penetration of these sensors in the global market has not yet occurred as the technology is competing with traditional sensors in terms of cost and production volume. The main challenges, not yet fully addressed, concern the manufacturing, integration and installation of the FBG sensors [7]–[8] as well as the development of compact and low cost interrogation systems.

Manuscript received 10 March 2022; revised 27 April 2022; accepted 4 May 2022. Date of publication 12 May 2022; date of current version 2 August 2022. This work was supported by Italian Ministry of Research and University (MIUR): special funding for the Departement of excellence in robotics and artificial Intelligence. *(Corresponding author: Stefano Faralli.)*

The authors are with the Institute of Mechanical Intelligence, Scuola Superiore Sant'Anna, 56124 Pisa, Italy and also with the Department of Excellence in Robotics & AI, Scuola Superiore Sant'Anna, 56127 Pisa, Italy (e-mail: l.tozzeti@santannapisa.it; f.bontempi@sssup.it; anna.giacobbe@santannapisa.it; f.dipasquale@sssup.it; stefano.faralli@santannapisa.it).

Color versions of one or more figures in this article are available at https://doi.org/10.1109/JLT.2022.3174770.

Digital Object Identifier 10.1109/JLT.2022.3174770

In particular, the need for FBG sensors readout units ensuring low size, weight, power consumption and cost (SWAP-C) is of strategic importance for industrial sectors such as automotive, aerospace and transport and these features cannot be fully satisfied by the use of bulk components. FBG interrogators based on photonic integrated circuits (PIC) can fulfill the challenges providing a sensing technology readily applicable for large volume and competitive with respect to traditional sensors in terms of cost and production volume [9].

The Silicon on Insulator (SOI) platform is the most attractive technology to produce high density and miniaturized PIC for sensing and communications applications [10]; its compatibility with CMOS processes allows full integration of electronic and photonic devices, making SOI technology the best candidate for mass-volume, low-cost fabrication of FBG interrogators.

Several integrated solutions for FBG sensor interrogation have been recently proposed on SOI platforms, either based on interferometric techniques or optical filters such as Echelle Grating, Arrayed Waveguide Grating (AWG) and ring resonator (RR). In [11] we demonstrated a wavelength division multiplexed FBG interrogator using an unbalanced Mach-Zehnder interferometer followed by an AWG integrated on a SOI platform; the use of a phase generated carrier demodulation technique permits an accurate measurement of the phase difference between the signal in each arm of the MZI and provides a minimum detectable strain of 0.5 $\mu\varepsilon$. The AWG and the Echelle Grating were also used as passband filter for integrated FBG interrogation systems [12]–[13], demonstrating their potential for multichannel interrogators with a wavelength resolution lower than 1 pm. However, their performances are affected by the fixed and limited number of output channels as well as in terms of the sensing range, number of interrogated FBG sensors, manufacturing yield and compactness. On the other hand, optical ring resonators can also be used for FBG interrogation; they are simple and compact optical passband filters characterized by great wavelength selectivity and flexible tunability of the wavelength resonance. FBG interrogators on chip based on ring resonators were reported in [14]–[15], where the wavelength shift of the FBG sensor is tracked by periodically tuning the resonant wavelength of the ring resonator; the FBG wavelength shift can be detected by the peak light intensity at the system output.

Since in such a scheme the resonance wavelength of the ring resonator is thermally tuned by an integrated heater, the heater

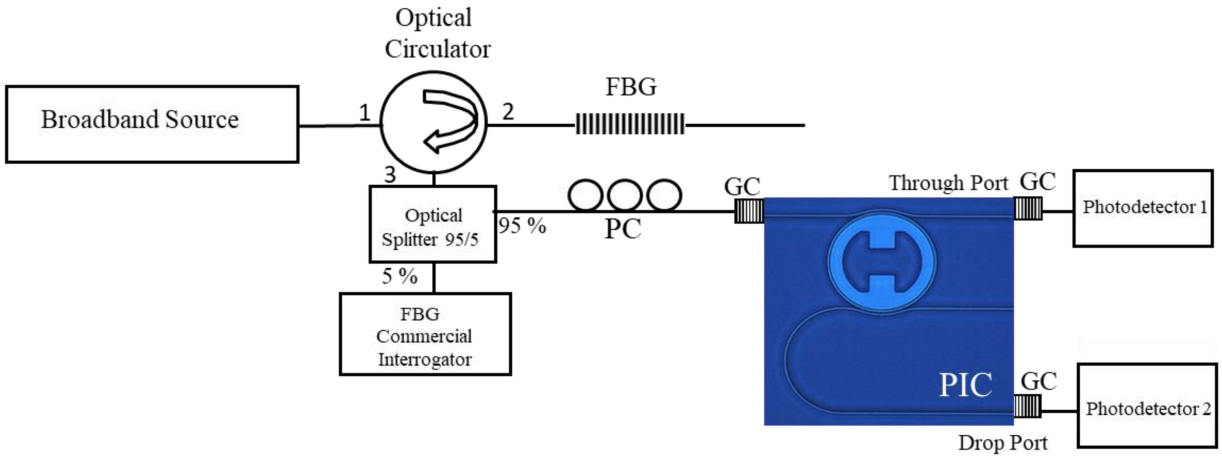

Fig. 1. Schematic diagram of the FBG interrogation system based on a SOI ring resonator. The figure includes a microscope picture of the SOI ring resonator. (PC: Polarization Controller; GC: Grating Coupler; PIC: Photonic Integrated Circuits; FBG: Fiber Bragg Grating)

time response limits the speed of the wavelength resonance scanning and the corresponding speed of the interrogation scheme. A phase detection method based on RRs using a dithering signal was also proposed in [16], where the generation of an antisymmetric error signal curve is used for locking the RR resonance to the FBG sensor wavelength shift. In order to overcome the speed limitation of such a sensor interrogator, the use of the non-linear transient response of a thermally tuned silicon ring resonator has been proposed in [17], however with some limitations mainly due to reliability issues related to possible micro-heater failure when operated at high frequency and power levels, and rather limited resolution. Note that an improved resolution would require a more accurate and reliable control of the non-linear transient response time of the RR heater.

In this work we propose a simple and effective method for FBG sensor wavelength shift measurement based on the direct detection of the signal intensity at the drop port of a ring resonator. The resonance wavelength of the ring resonator is first thermally tuned and then kept fixed at a given value which allows the ring resonator to convert the FBG wavelength shift into optical intensity variations at the drop port, with high dynamic capabilities. The speed of the proposed on chip FBG interrogator is only limited by the electrical bandwidth of the photodetector and extremely fast dynamic strain variations can be detected by the proposed interrogation method.

Note that there are specific applications for automotive components [18] and for non-destructive inspection of mechanical components by ultrasound waves [19]–[20] which require very large dynamic bandwidth [21] as well as integrated reading units suitable for mass production.

This paper first presents a theoretical analysis of the interrogation scheme that allows to predict the minimum detectable wavelength shift of the proposed FBG interrogator as a function of the ratio of the FBG spectrum bandwidth to the ring resonator passband bandwidth. Theoretical predictions in static conditions are well confirmed by the experimental results. A single FBG was then interrogated using two different ring resonators with different resonance bandwidths, demonstrating high speed dynamic measurement capabilities up to 40 kHz. The dynamic measurements were also compared with a commercial interrogator up to the frequency allowed by the commercial unit. The scalability of the interrogation scheme to a larger single FBG wavelength range and for wavelength division multiplexing of several FBG sensors has been theoretically investigated considering an array of cascaded ring resonators.

II. FBG Interrogation Method Based on a SOI Ring Resonator ADD/DROP Filter

A. Interrogation Method

The interrogation scheme based on the add/drop ring resonator (RR) is described in Fig. 1. The broadband light emitted by a superluminiscent LED is sent to port 1 of a three-port optical circulator (OC), while port 2 is connected to the FBG sensor. The light reflected by the FBG is coupled to port 3 of the OC and split by a 95/5 optical coupler. The 5% of the signal has been sent to the commercial read out unit Ibsen I-MON 512 USB for validating the proposed interrogation system, while the 95% of the signal is coupled to the PIC input port through a grating coupler after a polarization controller (PC). The filtered signals at the drop and through ports of the RR are coupled to external InGaAs photodiodes (PD) followed by trans impedance amplifiers with suitable bandwidth. Note that, unlike what is reported in this work, the PDs can be also integrated in the PIC by using integrated Ge photodetectors [22].

B. Theoretical Analysis of the Interrogation Method

The reflected FBG spectrum is passband filtered by the drop port of the ring resonator and detected by a photodetector coupled at the PIC output. The optical power detected at the drop output depends on the reflected spectrum of the FBG and the ring resonator resonance spectrum, allowing to detect the FBG wavelength peak shift. The optical power at the drop PD port is calculated as the integral over wavelength of a convolution profile as described by the following equation:

$$P_{PD}\ (\lambda_{FBG}) = \int_{-\infty}^{+\infty} H_{ring}\,(\lambda', \lambda_{RR}, \Delta\lambda)$$

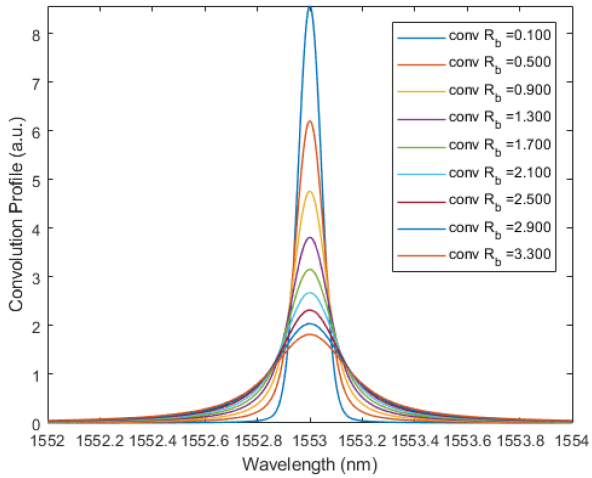

Fig. 2. Convolution profiles for different R_b values.

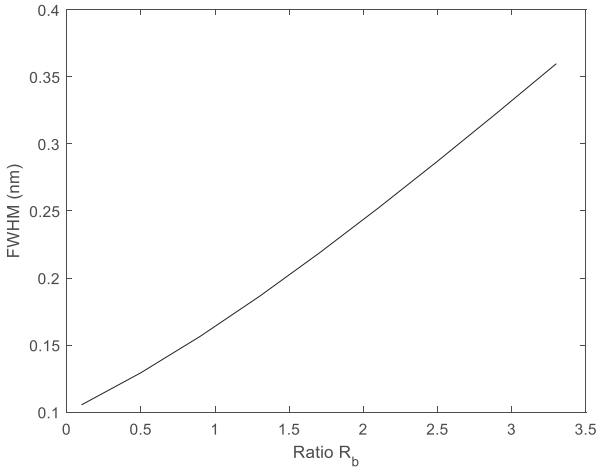

Fig. 3. Full Width Half Maximum FWHM of the convolution Voigt profile vs the ratio R_b.

$$R_{FBG}\left(\lambda_{FBG}-\lambda', B\right)\, d\lambda' \tag{1}$$

where H_{ring} is the spectral transfer function of the ring resonator and R_{FBG} is the reflection spectral response of the FBG, also including total power attenuation due to the insertion loss of the optical components such as OC, optical fiber, splitter and the PIC coupling loss. The wavelength shift of the FBG is tracked by the power variation at the drop port of the micro ring resonator which is kept at a fixed resonance wavelength λ_{RR}. Note that the RR transfer function at the drop port has a Lorentzian spectrum characterized with a 3-dB bandwidth $\Delta\lambda$, while we assume a Gaussian profile for the FBG spectrum with a 3-dB bandwidth B [23]. The resulting convolution spectrum corresponds to the total optical powers at the PD and depends on the main features of the convolved spectra. For implementing a general analysis of the FBG interrogator we have calculated the power detected at the RR drop port through (1) as a function of the ratio $R_b = \Delta\lambda/B$ between the 3-dB bandwidth of the ring resonator $\Delta\lambda$ and the FBG 3-dB bandwidth B.

Fig. 2 reports a comparison of the detected convolved spectral Voigt profiles for different R_b ratio values where both the spectra H_{ring} and R_{FBG} are normalized to their peak values. As an example, the H_{ring} spectral function is centered at 1553 nm and the drop PD output power is calculated as function of the λ_{FBG} wavelength peak position supposing a 3-dB bandwidth B = 100 pm. As shown in Fig. 3 the full width half maximum (FWHM) of the Voigt spectrum depends on the R_b ratio. For increasing values of the ratio R_b the FWHM amplitude of the convolution spectrum increases, the sharpness of the spectrum is reduced, and the convolution curve is turning into a more flattened profile. Figs. 2 and 3 provide useful information for the interrogator design: the maximum detected power is obtained for $\lambda_{FBG} = \lambda_{RR}$ but the perfect overlapping of the two spectral wavelength peak corresponds also to the stationary point of the Voigt profile. On the contrary by tuning the ring resonance at the wavelength corresponding to the maximum slope of the FBG reflected spectrum on the rising or falling fronts, it is possible to track the FBG wavelength shift by measuring the power variation at the drop port of the RR. Note that in order to maximize the

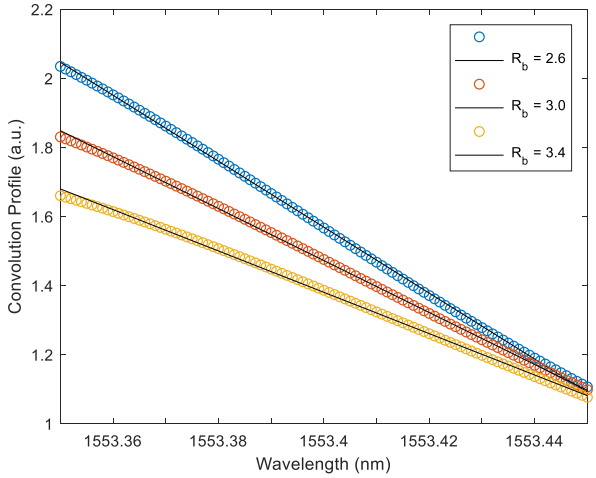

Fig. 4. Falling zone of the convolution spectra for different R_b.

detection sensitivity of the system, we must consider wavelength detection zones characterized by the highest slope of the detected signal. Fig. 4 shows a detail of Fig. 2 outlining the convolution profiles in the falling zones of the spectra calculated by Eq. 1 for different ratio Rb; the figure also includes linear fitting graphs (black line) for each convolution profile (colored marker). The slope of the linear fit is calculated in a wavelength range that provides a determination coefficient R^2 of the linear regression equal to 0.98.

Note that the slope of the linear regression decreases as the ratio R_b increases and is directly related to the interrogation detection range and sensitivity: high values of R_b correspond to a slope reduction with a larger detection range but lower sensitivity. In order to evaluate the interrogator sensitivity, we have calculated the minimum detectable wavelength shift as the minimum power variation that can be detected at the photodetector over the noise power level. The minimum detectable shift

TABLE I
PARAMETERS USED FOR THE MINIMUM DETECTABLE WAVELENGTH SHIFT EVALUATION

NEP	Noise equivalent power	1.25×10^{-12} W/$\sqrt{\text{Hz}}$
BW	electrical bandwidth of the PD	775 kHz
λ_{RR}	RR resonance wavelength	1553 nm
B	FBG Bandwidth	0.10 nm
R_b	Ratio Range	0.1-3.4

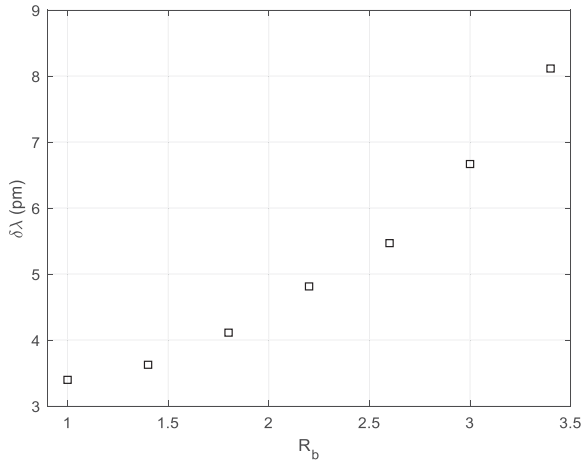

Fig. 5. Minimum detectable wavelength shift vs the ratio R_b.

$\delta\lambda$ has been computed using the following equation:

$$\delta\lambda = \frac{NEP(\lambda) \cdot \sqrt{BW}}{S(R_b)} \tag{2}$$

where NEP is the noise equivalent power of the photodetector, BW is the photodiode electrical bandwidth and S is the slope of the linear regression of the convolution profile.

In order to compare theoretical and experimental results we have considered an FBG sensor with a central wavelength peak at 1553 nm, a 3-dB Gaussian bandwidth B = 100 pm, and a reflectivity of 25%; the RR filters, characterized by Lorentzian profiles, have been fabricated with variable 3-dB bandwidths $\Delta\lambda$. Table I shows the parameters used for the minimum detectable wavelength shift evaluation, while Fig. 5 shows the minimum detectable wavelength shift for different ratio R_b corresponding to different FWHM of the convolution detection spectrum.

The results of Fig. 5 confirm that higher sensitivity values correspond to lower FWHM, lower R_b values, and sharper convolution profiles.

III. DESIGN FABRICATION AND CHARACTERIZATION OF THE SOI RING RESONATOR

In order to experimentally demonstrate the interrogation method two different integrated ring resonators have been fabricated and used in the experimental set up of Fig. 1. The ring resonators were fabricated at the Institute of Microelectronics (IME), Singapore, in a multi-project wafer run on a 220-nm

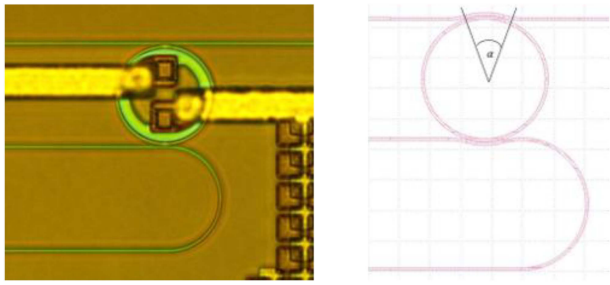

Fig. 6. Microscope picture of the SOI add/drop ring resonator, and the corresponding RR layout.

Silicon on Insulator platform. The add/drop ring resonators have a radius of 10 μm; the cross section of the ring consists of a 480-nm-wide single-mode half-rib waveguide, and the wavelength tuning is obtained by exploiting the Joule effect induced by electrical current injection in the doped 90-nm-thick internal slab [24]–[26]. The input and output ports, corresponding to the dropped and through signals, are coupled to single mode fibers by two single-polarization transverse electric (TE) grating couplers.

Note that parameters fabrication errors can affect the response of wavelength dependent integrated devices such as RR filters and must be in general considered in the design phase. In particular, scanning electron microscopy and ellipsometry based techniques can respectively evaluate the waveguides width and the thickness of the SOI layer with good accuracy during the fabrication process [27]. These geometrical variations can also be accurately mapped through the wafer using non-destructive characterization methods, as described in [28]. Although significant deviations are expected on the resonant wavelengths of the designed RR filters [29], in our specific application we can easily compensate them by thermally tuning the ring resonator resonance to the linear region of the specific FBG sensor. This tuning can be interpreted as a calibration procedure which is done to fix the resonance wavelength at a given value allowing the RR filter to convert FBG wavelength shift into optical intensity variations. Note that spurious temperature variations are minimized by controlling the chip temperature through Peltier thermoelectric cooling.

One of the fabricated add-drop ring resonators with the integrated heater is shown in Fig. 6: unlike usual straight bus waveguide, the fabricated devices include bent bus waveguides to increase the coupling region. As shown in the ring resonator layout on the right side of Fig. 6, the bending arc length can be controlled by the angle α at the center of the ring; note that the more the arc length increases, the more the coupling region will be extended resulting in a higher coupling coefficient and a corresponding larger bandwidth.

As reported in Table II, two ring resonators with two different coupling ratios and 3-dB bandwidths have been fabricated and used for evaluating the interrogation method performance. The spectral characterization of the ring resonators was done at room temperature using a continuous wave external cavity tunable laser in the range between 1500 nm and 1600 nm; the signal is coupled to the RR using an input grating coupler and a

TABLE II
RING RESONATORS' CHARACTERISTICS

Ring Resonator	Ring Radius	FSR	Coupling Ratio	FWHM Bandwidth
Ring 1	10 um	9.5 nm	0.120	400 pm
Ring 2	10 um	9.5 nm	0.039	120 pm

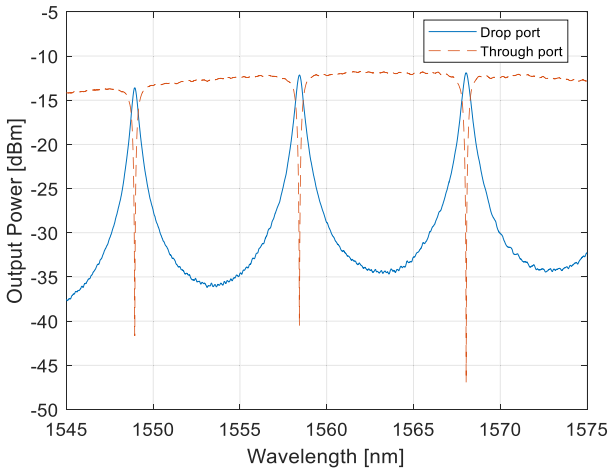

Fig. 7. Drop and Through port spectra of the ring resonator 1.

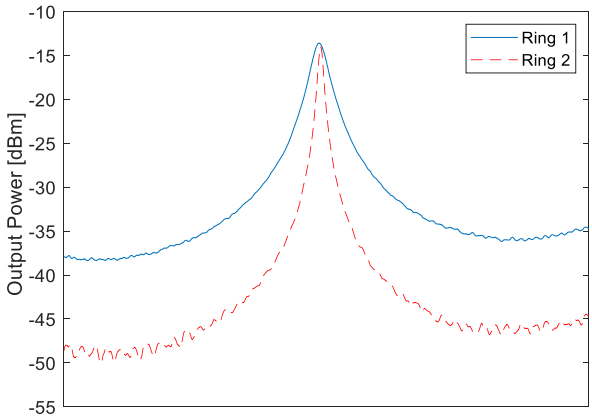

Fig. 8. Overlapped spectra at the drop port of the ring resonators.

polarization controller (PC) and the output spectra are acquired with a synchronized power meter.

Fig. 7 reports the spectral responses measured at the through and drop ports of the ring resonator 1, while Fig. 8 shows the overlapped spectra at the drop port of the two ring resonators.

Note that the free spectral range of the RR filters is 9.2 nm allowing the use of cascaded RR filters to interrogate a single FBG sensor over a large interrogation range or multiplexed FBG sensors, as it will be shown in Section V.

The resonance wavelength shift of the two rings with respect to the electrical dissipated power applied to the heater has been characterized by applying different current values to the integrated heater and is shown in Fig. 9; the obtained tuning

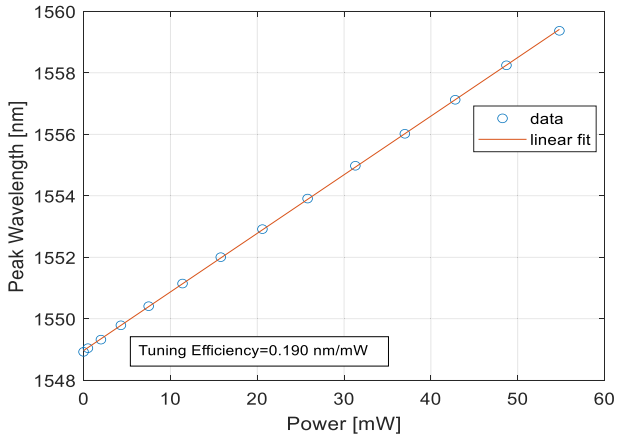

Fig. 9. Ring Resonance wavelength as function of the electrical power applied to the ring heater.

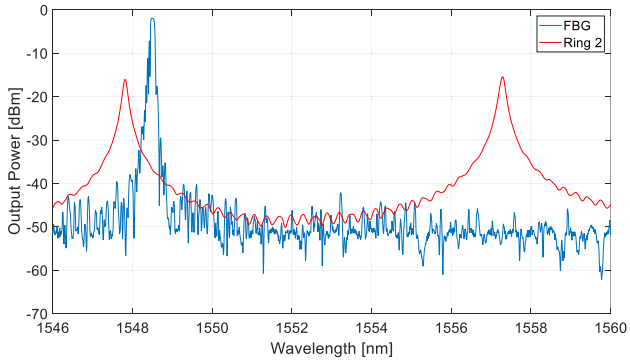

Fig. 10. FBG (blue line) and ring resonator 2 (red line) spectra.

efficiency is 190 pm/mW and a full Free Spectral Range (FSR) wavelength shift is obtained for an applied electrical power of 50 mW.

IV. EXPERIMENTAL RESULTS

The performance of the FBG interrogator on chip has been evaluated by using the two different ring resonators previously characterized; Table II reports the FWHM of the two ring resonators that correspond to two different ratio values R_b, where the 3-dB bandwidth of the FBG sensor is 100 pm. In order to characterize both static and dynamic behaviors with the same experimental set-up, we used an IDIL tunable Fiber Bragg Grating sensor where the FBG is fixed on a piezoelectric (PZT) stack and an elongation of the FBG is created by applying an electric voltage on the PZT actuator. The piezoelectric stack makes the wavelength behavior of the FBG weakly sensitive to temperature variations with a wavelength drift less than 100 pm between -20 °C and 70 °C; moreover, all the tests were carried out at controlled constant room temperature.

The spectra of Fig. 10 have been measured by sweeping the wavelength of the continuous wave external cavity tunable laser, and the output spectra are taken with a synchronized power meter. Fig. 10 shows the FBG (blue line) and ring resonator 2 (red line) spectra.

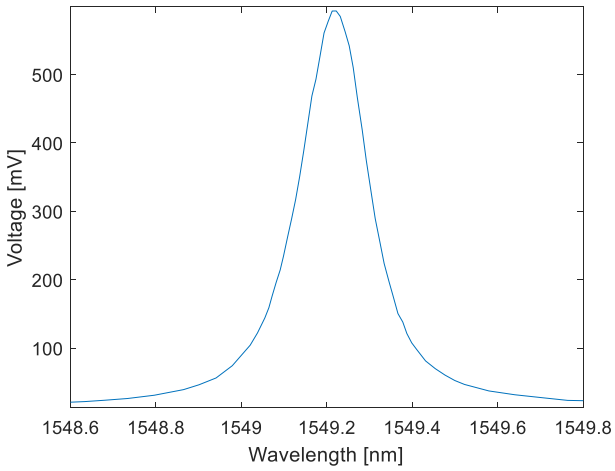

Fig. 11. Ring Resonance 2 drop output voltage vs the FBG wavelength central peak.

TABLE III
STATIC AND DYNAMIC CHARACTERISTICS OF THE FBG INTERROGATORS FOR TWO DIFFERENT RING RESONATORS

		DSR	DSR	DSR
RR	δλ	100 Hz	1 kHz	40 kHz
Ring 1	6.18 pm	3.7 nε/√Hz	3.2 nε/√Hz	2.9 nε/√Hz
Ring 2	3.3 pm	5.8 nε/√Hz	3.1 nε/√Hz	1.3 nε/√Hz
Com. Interr.	8.7 pm	42 nε/√Hz	67 nε/√Hz	

$\delta\lambda$: Static Measurement Precision. DSR: Dynamic Strain Resolution; RR: Ring Resonator.

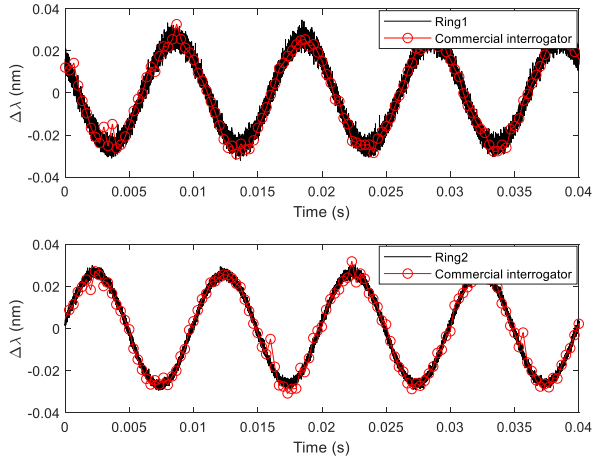

Fig. 12. Comparison of measured wavelength variation versus time at 100 Hz obtained by the ring resonators and the commercial read out unit.

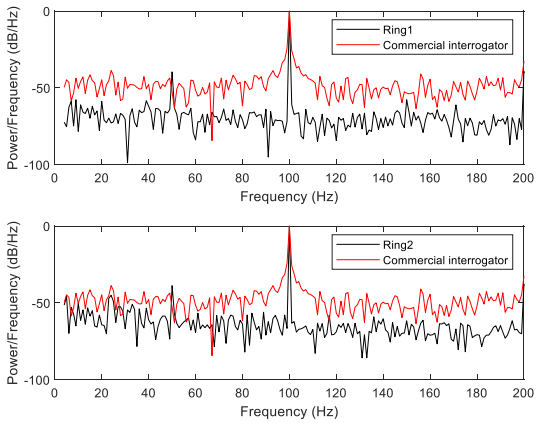

Fig. 13. Power Spectral Density of the measured wavelength variation signals for the two ring resonators and the commercial read out unit at 100 Hz

According to the experimental set up of Fig. 1, where the FBG is interrogated by a broadband source, Fig. 11 reports the voltage measured by the photodetector at the RR2 drop port versus the FBG wavelength central peak, corresponding to different static strains applied to the FBG; the maximum detected voltage is obtained for $\lambda_{\mathrm{FBG}} = \lambda_{\mathrm{RR}}$ and the measured values reported in the figure reconstruct the convolution of the spectral responses of the RR and FBG spectra as described by (1).

In order to have the best sensitivity and evaluate the dynamic behaviors of the interrogation method, the RR wavelength has been tuned and then kept constant in the linear zone of the unstrained FBG spectral profile; then the FBG has been dynamically strained and the corresponding induced wavelength shift has been compared with the one measured by a commercial interrogator for comparison. The minimum detectable wavelength shifts $\delta\lambda$ reported in Table III are measured as 3σ, where σ is the standard deviation of the fluctuations detected for the FBG reflected spectrum at a given wavelength, without applying any signal to the piezo actuator. As previously theoretically discussed, $\delta\lambda$ depends on the ratio between the FBG and the RR bandwidths and the electrical noise source at the PD, and the measured $\delta\lambda$ for the two rings ranges between 3.3 pm and 6.2 pm for an increasing value of the ring resonator bandwidth. Note that the long term stability of the used Peltier controller ensures a temperature stability of the chip less than 0.1 °K, leading to a negligible error in the wavelength shift measurement, lower than 1 pm.

In order to perform the dynamic characterization of the chip interrogator and compare its performance with a commercial reading unit, low frequency periodic strain variations have been first applied to the FBG through the piezo actuator driven by sinusoidal electrical waveforms at 100 Hz and 1 kHz, while the RR resonance wavelength was tuned at the maximum slope wavelength of the FBG reflected spectrum. Measurement at 40 KHz have been performed only with the integrated reading unit.

Fig. 12 shows a comparison of a ∼50 pm peak to peak wavelength variation at 100 Hz, measured by the two RRs and by the commercial interrogator; Fig. 13 reports the corresponding power spectral densities. The signal-to-noise ratio normalized at 1 Hz bandwidth for the two ring resonators RR1 and RR2 is respectively 72.13 dB and 68.62 dB and results in a corresponding dynamic strain resolution of 3.7 $n\varepsilon/\sqrt{\mathrm{Hz}}$ and 5.8 $n\varepsilon/\sqrt{\mathrm{Hz}}$, while for the commercial interrogator the signal-to-noise ratio normalized at 1 Hz bandwidth is 51.02 dB and results in a dynamic strain resolution of 42 $n\varepsilon/\sqrt{\mathrm{Hz}}$. As expected the reduction of the ratio R_b corresponds not only to a higher minimum detectable wavelength shift but also to a lower dynamic strain resolution. Note that the commercial reading unit is a spectrometer based on fused silica transmission

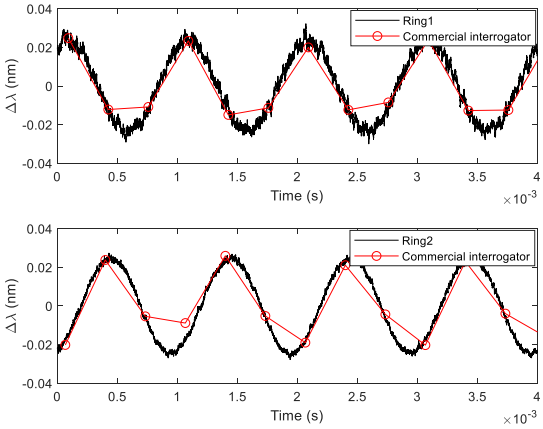

Fig. 14. Comparison of measured wavelength variation versus time at 1 kHz obtained by the two ring resonators and the commercial read out unit.

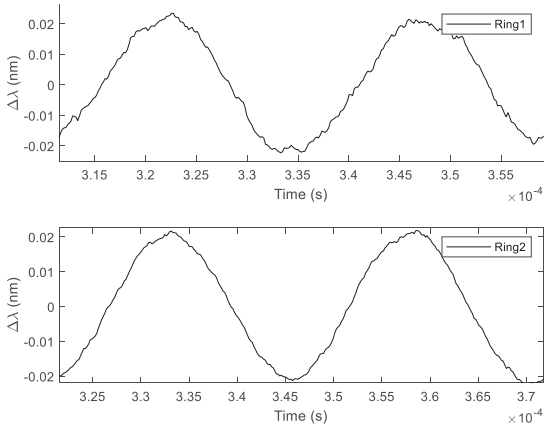

Fig. 16. Measured wavelength variation versus time at 40 kHz obtained by the two ring resonators.

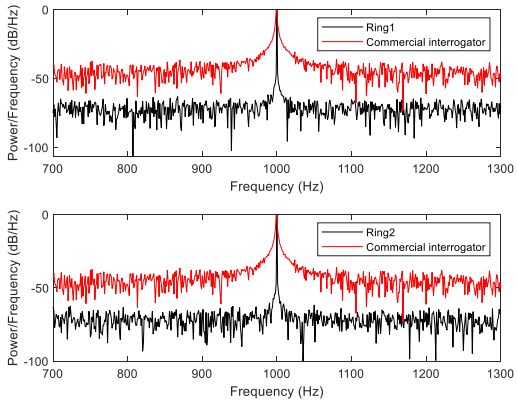

Fig. 15. Power Spectral Density of the measured wavelength variation signal for the two ring resonators and the commercial read out unit at 1 kHz.

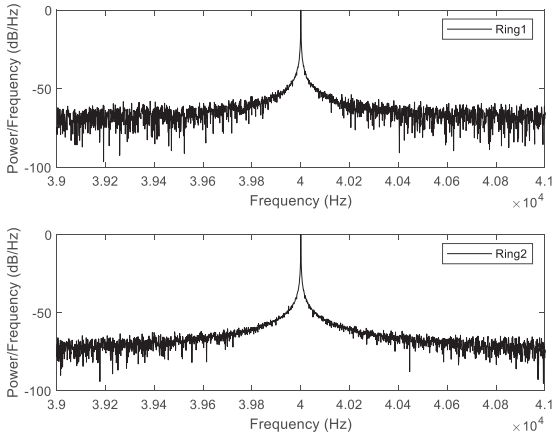

Fig. 17. Power Spectral Density of the measured wavelength variation signal for the two ring resonators at 40 kHz.

gratings that spatially split the wavelength spectrum measured by a photodiode array, that limits the maximum measurement frequency to 3 kHz.

In order to evaluate the interrogator at higher frequency but still achievable by the commercial reading unit, a FBG wavelength variation of ∼50 pm has been applied at 1 kHz. Figs. 14 and 15 report respectively the wavelength variations versus time and the corresponding power spectral densities for the two different ring resonators and the commercial interrogator at 1 kHz: the signal-to-noise ratio normalized at 1 Hz bandwidth for the RR1 and RR2 is respectively 73.03 dB and 73.81 dB leading to a dynamic strain resolution of 3.2 n$\varepsilon/\sqrt{\text{Hz}}$ and 3.1 n$\varepsilon/\sqrt{\text{Hz}}$. For the commercial interrogator the signal-to-noise ratio normalized at 1 Hz bandwidth is reduced to 46.04 dB, resulting in a dynamic strain resolution of 67 n$\varepsilon/\sqrt{\text{Hz}}$. As expected, a higher interrogation frequency corresponds to a degradation of the commercial interrogator dynamic strain resolution due to its limited measurement frequency bandwidth.

In order to test the interrogation method at extremely high frequencies an FBG wavelength sinusoidal variation of 40 pm has been applied at 40 kHz; Figs. 16 and 17 report the wavelength variation and the power spectral density for the two ring resonators. Note that the maximum stress frequency that could be applied to FBG sensor was limited by the frequency response of the piezo actuator; also we did not observe any performance degradation of the RR based integrated interrogation method as its dynamic performance is basically only limited by the electrical bandwidth of the used Thorlabs PDA10CS InGaAs Switchable Gain photodetector (775 KHz with an electrical gain of 2.38 x 10^4 V/A).

Figs. 16 and 17 clearly point out the fast capabilities of the proposed integrated reading unit on chip, demonstrating its potential for fast dynamic strain measurement.

Table III resumes the performance of the integrated interrogators in static and dynamic conditions and the comparison with the performance of the commercial interrogator.

V. Multi Ring Interrogation

In the previous chapters we have proposed an FBG interrogation method based on a ring resonator which is initially thermally tuned to the linear slope region of the FBG sensor and then kept fixed at a given resonance wavelength, allowing the ring resonator to convert the FBG wavelength shift into optical intensity variations at the RR drop port. The range of the FBG interrogation is limited and is determined by the rising and falling zones of the convolution spectrum as reported in Fig. 4.

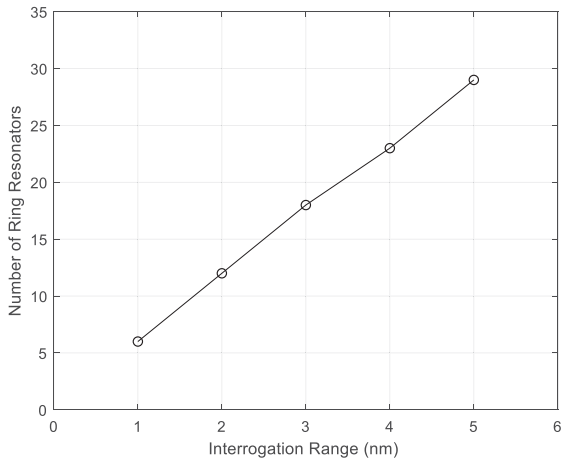

Fig. 18. Ring resonator number of a multi-ring interrogation system vs the interrogation range for R_b=3.0.

In order to scale into a larger interrogation range, an interrogation system based on a ring resonator array can be designed where every single resonance wavelength of the RRs is tuned in order to monitor a dedicated zone of the FBG wavelength shift range. In a multi-ring interrogation system, a single bus waveguide is coupled to the ring resonator cascade and the optical power at the drop ports is detected by an array of integrated photodiodes. The simultaneous monitoring of the output photo-detected electrical signals can be implemented by a read out electrical front end where an electronic ASIC is directly connected to the photonic chip by wire bonding or flip chip electrical connections; note that the integration of the electrical and photonic circuits allows for simple and effective multichannel operations in a reduced footprint [30].

As discussed in chapter II the range of the FBG interrogation and the corresponding minimum detectable shift mainly depend on the 3-dB bandwidth of the ring resonator $\Delta\lambda$, the FBG 3-dB bandwidth B and the ratio $R_b = \Delta\lambda/B$; in a multi-ring configuration the number of the ring resonators required for interrogating a given FBG sensor moving its Bragg wavelength peak over a given wavelength range will increase for lower R_b values. Fig. 18 reports the calculated number of ring resonators vs the FBG interrogation wavelength range for $R_b = 3.0$, where we have assumed to equally space the RR resonance wavelengths; the number of ring resonators linearly increases with the interrogation range. Note that the multi ring scheme can be effectively used for fast interrogation of a single FBG moving over a very large wavelength range, as required in specific applications, as well as for fast WDM interrogation of multiplexed FBG sensors. The RR filters along the cascade require dedicated photodetectors which can however be integrated on the chip.

Also note that in case of WDM FBG sensors in order to avoid multiple peak detections on a single photodetector, the free spectral range of the ring resonators limits the maximum interrogation range: the FSR of the micro rings reported in this paper with 10 μm ring radius limits the interrogation range to 9.2 nm. However suitable schemes can be designed using integrated array waveguide grating (AWG) devices on chip to separate the different WDM channels before introducing cascaded micro-ring resonators on each of them. Depending on the application, the design of the multi-ring interrogation system can be based on a flexible approach where a configuration with variable resonance wavelength spacing and bandwidth of the ring resonators can be adopted on the same array of ring resonators.

VI. Conclusion

We presented an on chip FBG interrogator based on the wavelength shift detection by a ring resonator add drop filter. The chip was fabricated on a Silicon on Insulator platform and allows for accurate and high speed FBG interrogation. The experimental comparison with a commercial interrogator demonstrates a good agreement and provides a validation of the measurement technique. Experimental results with high frequency dynamic strain up to 40 kHz does not show any performance degradation, that is only limited by the photodetector bandwidth.

Note that by integrating array waveguide gratings and photodetectors on chip would further improve the performance of the proposed integrated interrogator allowing for fast interrogation of wavelength multiplexed FBG sensors and paving the way to mass-volume applications of the FBG technology.

References

[1] Y. Zhang, S. Li, Z. Yin, B. Chen, H.-L. Cui, and J. Ning, "Fiber-Bragg-grating-based seismic geophone for oil/gas prospecting," *Opt. Eng.*, vol. 45, no. 8, Aug. 2006, Art. no. 084404, doi: 10.1117/1.2337631.

[2] M. Majumder *et al.*, "Fibre Bragg gratings in structural health monitoring—Present status and applications," *Sensors Actuators A: Phys.*, vol. 147, no. 1, pp. 150–164, 2008.

[3] P. Velha *et al.*, "Monitoring large railways infrastructures using hybrid optical fibers sensor systems," *IEEE Trans. Intell. Transp. Syst.*, vol. 21, no. 12, pp. 5177–5188, Dec. 2020, doi: 10.1109/TITS.2019.2949752.

[4] G. Honglei *et al.*, "Fiber optic sensors for structural health monitoring of air platforms," *Sensors*, vol. 11, no. 4, pp. 3687-3705, 2011.

[5] P. Tripicchio, S. D'Avella, C. A. Avizzano, F. Di Pasquale, and P. Velha, "On the integration of FBG sensing technology into robotic grippers," *Int. J. Adv. Manuf. Technol.*, vol. 111, pp. 1173–1185, 2020, doi: 10.1007/s00170-020-06142-8.

[6] L. Tozzetti *et al.*, "Fiber Bragg grating sensors for dynamic strain measurements in gasoline direct injectors," *IEEE Trans. Veh. Technol.*, vol. 70, no. 6, pp. 5658–5668, Jun. 2021, doi: 10.1109/TVT.2021.3081363.

[7] G. G. Kuhn, K. M. Sousa, C. Martelli, C. A. Bavastri, and J. C. C. D. Silva, "Embedded FBG sensors in carbon fiber for vibration and temperature measurement in power transformer iron core," *IEEE Sensors J.*, vol. 20, no. 22, pp. 13 403–13 410, Nov. 2020, doi: 10.1109/JSEN.2020.3005884.

[8] G. Xue, X. Fang, X. Hu, and L. Gong, "Measurement accuracy of FBG used as a surface-bonded strain sensor installed by adhesive," *Appl Opt.*, vol. 57, no. 11, pp. 2939–2946, Apr. 2018, doi: 10.1364/AO.57.002939.

[9] W. Shi, Ye Tian, and A. Gervais, "Scaling capacity of fiber-optic transmission systems via silicon photonics," *Nanophotonics*, vol. 9, no. 16, pp. 4629–4663, 2020, doi: 10.1515/nanoph-2020-0309.

[10] L. C. Kimerling *et al.*, *Electronic-Photonic Integrated Circuits on the CMOS Platform*, Bellingham, WA, USA: SPIE, 2006.

[11] Y. E. Marin *et al.*, "Integrated dynamic wavelength division multiplexed FBG sensor interrogator on a silicon photonic chip," *J. Lightw. Technol.*, vol. 37, no. 18, pp. 4770–4775, Sep. 2019.

[12] A. Trita *et al.*, "Simultaneous interrogation of multiple fiber bragg grating sensors using an arrayed waveguide grating filter fabricated in SOI platform," *IEEE Photon. J.*, vol. 7, no. 6, pp. 1–11, Dec. 2015, Art. no. 7802611, doi: 10.1109/JPHOT.2015.2499546.

[13] H. Li *et al.*, "Chip-scale demonstration of hybrid III–V/silicon photonic integration for an FBG interrogator," *Optica*, vol. 4, pp. 692–700, 2017.

[14] A. Shen *et al.*, "Tunable microring based on-chip interrogator for wavelength-modulated optical sensors," *Opt. Commun.*, vol. 340, pp. 116–120, 2015.

[15] G. R. Vargas and R. R. Panepucci, "Wavelength monitoring using a thermally tuned micro-ring resonator," *Numer. Simul. Optoelectron. Devices*, 2010, pp. 83–84.
[16] F. Yang, W. Zhang, S. Zhao, Q. Liu, J. Tao, and Z. He, "Miniature interrogator for multiplexed FBG strain sensors based on a thermally tunable microring resonator array," *Opt. Exp.*, vol. 27, pp. 6037–6046, 2019.
[17] H.-T. Kim and M. Yu, "High-speed optical sensor interrogator with a silicon-ring-resonator-based thermally tunable filter," *Opt. Lett.*, vol. 42, pp. 1305–1308, 2017.
[18] L. Tozzetti *et al.*, "Fiber Bragg grating sensors for dynamic strain measurements in gasoline direct injectors," *IEEE Trans. Veh. Technol.*, vol. 70, no. 6, pp. 5658–5668, Jun. 2021, doi: 10.1109/TVT.2021.3081363.
[19] S. Goossens *et al.*, "Spectral verification of the mechanisms behind FBG-based ultrasonic guided wave detection," *Sensors,* vol. 20, Nov. 2020, Art. no. 6571, doi: 10.3390/s20226571.
[20] A. Minardo, A. Cusano, R. Bernini, L. Zeni, and M. Giordano, "Response of fiber Bragg gratings to longitudinal ultrasonic waves," *IEEE Trans. Ultrasonics, Ferroelect. Freq. Control*, vol. 52, no. 2, pp. 304–312, Feb. 2005, doi: 10.1109/TUFFC.2005.1406556.
[21] C. J. Oton, L. Tozzetti, and F. D. Pasquale, "High-speed FBG interrogation with electro-optically tunable sagnac loops," *J. Lightw. Technol.*, vol. 38, no. 16, pp. 4513–4519, Aug. 2020, doi: 10.1109/JLT.2020.2991272.
[22] H. Li *et al.*, "Silicon waveguide integrated with germanium photodetector for a photonic-integrated FBG interrogator," *Nanomaterials*, vol. 10, 2020, Art. no. 1683, doi: 10.3390/nano10091683.
[23] D. TosI, "Review and analysis of peak tracking techniques for fiber Bragg grating sensors," *Sensors*, vol. 17, 2017, Art. no. 2368, doi: 10.3390/s1710236.
[24] F. Gambini *et al.*, "Experimental demonstration of a 24-port packaged multi-microring network-on-chip in silicon photonic platform," *Opt. Exp.*, vol. 25, pp. 22 004–22 016, 2017.
[25] S. Faralli *et al.*, "Bidirectional transmission in an optical network on chip with bus and ring topologies," *IEEE Photon. J.*, vol. 8, no. 2, Apr. 2016, Art. no. 0600407.
[26] P. Pintus *et al.*, "PWM-Driven thermally tunable silicon microring resonators: Design, fabrication, and characterization," *Laser Photon. Rev.*, vol. 13, no. 9, 2019, Art. no. 1800275.
[27] S. K. Selvaraja, W. Bogaerts, P. Dumon, D. Van Thourhout, and R. Baets, "Subnanometer linewidth uniformity in silicon nanophotonic waveguide devices using CMOS fabrication technology," *IEEE J. Sel. Top. Quantum Electron.*, vol. 16, no. 1, pp. 316–324, Jan./Feb. 2010.
[28] C. J. Oton, C. Manganelli, F. Bontempi, M. Fournier, D. Fowler, and C. Kopp, "Silicon photonic waveguide metrology using Mach-Zehnder interferometers," *Opt. Exp.*, vol. 24, pp. 6265–6270, 2016.
[29] C. Chauveau, P. Labeye, J. M. Fedeli, S. Blaize, and G. Lerondel, "Study of the uniformity of 300mm wafer through ring-resonator analysis," in *Proc. IEEE Int. Conf. Photon. Switching*, 2012, pp. 1–3. doi: 10.1109/JSTQE.2019.2945927.
[30] N. C. Abrams *et al.*, "Silicon photonic 2.5D multi-chip module transceiver for high-performance data centers," *J. Lightw. Technol.*, vol. 38, no. 13, pp. 3346–3357, Jul. 2020, doi: 10.1109/JLT.2020.2967235.

Lorenzo Tozzetti was born in Florence, Italy, in 1982. He received the bachelor's degree in physics and the master's degree in astrophysics from the University of Florence, Florence, Italy, in 2009 and 2017, respectively. From 2009 to 2011, he worked on the production of Cosmic Dust Analogs with the Department of Physics and Astronomy, University of Florence, as a Research Fellow. From 2011 to 2014, he was with the INAF - Astrophysical Observatory of Arcetri, Florence, Italy, as a Research Fellow, focusing on the characterization of Cosmic Dust Analogs. In the following two years, he further developed the same topics with the University of Florence. From 2016 to 2017, he was with the CNR - National Institute of Optics (INO), Florence, Italy, on the development of a prototype for the analysis of the composition of planetary atmospheres. Since 2018, he has been with TeCIP Institute, Scuola Superiore Sant'Anna, Pisa, Italy, as a Research Fellow, with particular interest on optical fiber sensors and silicon photonic.

Francesca Bontempi received the B.S. and M.S. degrees in telecommunications engineering from the University of Pisa, Pisa, Italy, in 2003 and 2007, respectively, and the Ph.D. degree from Scuola Superiore Sant'Anna, Pisa, Italy, in 2013. From 2014 to 2018, she was a Metrology Engineer with the Integrated Photonic Technologies Center of Scuola Superiore Sant'Anna, where she was an In-charge of the measurements of optical properties in thin-films and nanosized structures and the optical characterization of photonic integrated building blocks and devices for cleanroom process validation. She is currently a Technologist with Scuola Superiore Sant'Anna. Her research interests include modeling and design of optical integrated circuits, and characterization of integrated devices and systems for telecommunication and sensing.

Anna Giacobbe's biography is not available at the time of publication

Fabrizio Di Pasquale received the degree in electronic engineering from the University of Bologna, Bologna, Italy, in 1989, and the Ph.D. degree in information technology from the University of Parma, Parma, Italy, in 1993. From 1993 to 1998, he was with the Department of Electrical and Electronic Engineering, University College London, London, U.K., as a Research Fellow, working on optical amplifiers, WDM optical communication systems, and liquid crystal displays. After two years with Pirelli Cavi e Sistemi and two years with Cisco Photonics Italy, he moved to Scuola Superiore Sant'Anna, Pisa, Italy, where he is currently a Full Professor of telecommunications with the Institute of Mechanical Intelligence. He is the Co-founder of Infibra Technologies S.r.l., a spin-off company of Scuola Superiore Sant'Anna, developing and marketing fiber optic sensor systems. He has filed 24 patents and is author or coauthor of more than 240 scientific journals and conference papers. His research interests include optical fiber sensors, silicon photonics, optical amplifiers, WDM transmission systems, and networks. He has been the TPC member of several international conferences and on the Board of Reviewers of international refereed journals.

Stefano Faralli (Member, IEEE) received the M.Sc. degree in physics from the University of Pisa, Pisa, Italy, in 2000, the M.Sc. degree in optical communications systems and networks from the Politecnico di Milano, Milan, Italy, in 2001, and the Ph.D. degree in telecommunications technology from Scuola Superiore Sant'Anna, Pisa, Italy, in 2006. He is currently an Assistant Professor with Scuola Superiore Sant'Anna. In the period between 2011 and 2012, he was a Visiting Scholar with the Optoelectronics Group, University of California, Santa Barbara, CA, USA. In the period between 2015 and 2017, he was a Senior Process Engineer with the Inphotec center of Scuola Superiore Sant'Anna In-charge for the processes of PECVD and LPCVD deposition, wet and dry oxidation. He is also the Co-founder of Infibra Technologies S.r.l., a spin-off company of Scuola Superiore Sant'Anna. He is author or coauthor of publications among patens and papers in peer-reviewed international journals and conference digests. His research interests include optical fiber sensors, integrated optics, silicon photonics, thin film processing, and optical amplification for optical communication systems and networks.